THIS MONTH IN
JNM

Focus on preclinical SPECT: Peterson and Shokouhi offer perspectives on recent innovations in preclinical SPECT instrumentation, including new approaches to collimation, detection, acquisition geometry, calibration, and reconstruction. . . . . ***Page 841***

PET/MRI vs. PET/CT in cancer: Drzezga and colleagues look at areas of comparison in clinical performance between PET/CT and integrated whole-body PET/MRI in patients with oncologic diseases. . . . . ***Page 845***

PET/CT and cardiac tumors: Rahbar and colleagues explore the diagnostic utility of ^{18}F-FDG PET and the incremental value of an optimized CT score in preoperative assessment of malignancy of cardiac tumors. . . . . ***Page 856***

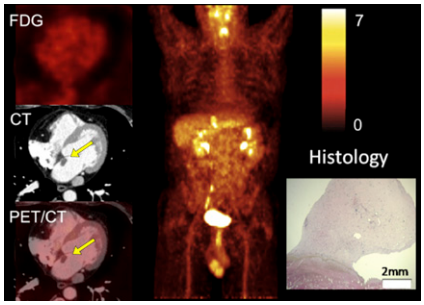

PET/CT in esophageal cancer staging: Barber and colleagues report on incremental information, management impact, and prognostic stratification provided by PET/CT in primary staging of esophageal cancer in a group of patients over an extended follow-up period. . . . . ***Page 864***

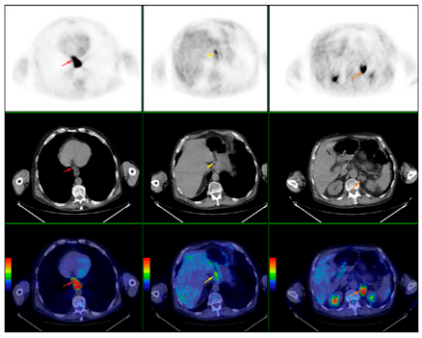

Therapy evaluation in esophageal cancer: Yanagawa and colleagues compare the PERCIST and RECIST response criteria in patients undergoing neoadjuvant chemotherapy for locally advanced esophageal cancer. . . . . ***Page 872***

PET and salivary duct carcinoma: Kim and colleagues assess the utility of ^{18}F-FDG PET and CT in preoperative staging, determination of neck node involvement, and surgical planning for patients with salivary duct carcinoma of the major salivary gland. . . . . ***Page 881***

Myocardial flow reserve in CKD: Fukushima and colleagues use ^{82}Rb PET/CT in evaluation of myocardial microcirculation in patients with chronic kidney disease, normal left ventricular function, and no flow-limiting coronary artery disease. . . . . ***Page 887***

3D SPECT scar models and ablation: Tian and colleagues assess the value of ^{201}Tl SPECT perfusion imaging to define ventricular myocardial scar areas and characterize myocardial substrate categories of scar, border zone, and normal myocardium. . . . . ***Page 894***

^{18}F-FDG and ^{18}F-florbetapir in AD: Newberg and colleagues compare clinical interpretations of the ^{18}F-labeled amyloid tracer florbetapir with those of ^{18}F-FDG PET in healthy volunteers and patients with Alzheimer disease. . . . . ***Page 902***

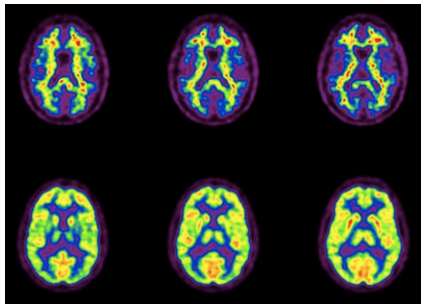

^{18}F-FP-(+)-DTBZ PET of β-cell mass: Normandin and colleagues evaluate this vesicular monoamine transporter type-2 agent for quantitative PET imaging of endogenous pancreatic β-cell mass in healthy individuals and patients with type 1 diabetes mellitus. . . . . ***Page 908***

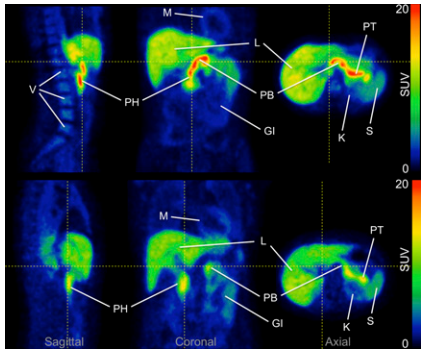

Exercise and muscle ^{18}F-FDG uptake: Lyall and colleagues describe the effects of treadmill exercise on ^{18}F-FDG uptake in skeletal muscles and image quality of torso PET and compare myocardial ^{18}F-FDG uptake with stress myocardial perfusion imaging patterns. . . . . ***Page 917***

Radretumab RIT in lymphoma: Erba and colleagues look at lesion uptake, safety, and clinical activity of L19SIP radioimmunotherapy in patients with relapsed lymphoma or multiple myeloma. ***Page 922***

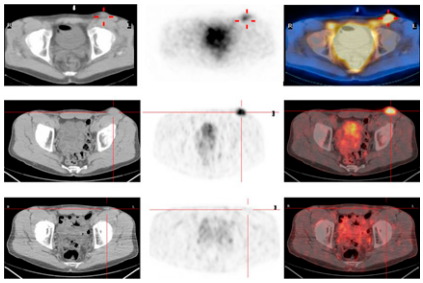

PET/MRI in oncology: Buchbender and colleagues provide an educational overview of early experience with PET/MRI in tumors of the brain, head and neck, chest, abdomen, and pelvis and outline the potential long-term implications for oncologic applications. ***Page 928***

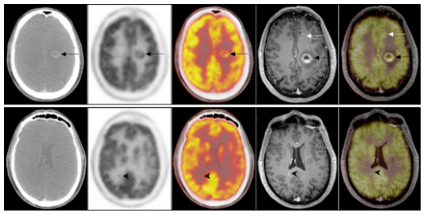

^{18}F-Affibody and HER2-positive metastases: Kramer-Marek and colleagues compare the use of a radiolabeled human epidermal growth factor receptor 2–specific Affibody and ^{18}F-FDG in HER2-expressing pulmonary metastases in a murine model of breast cancer. ***Page 939***

PET with ^{18}F-labeled bombesin analog: Dijkgraaf and colleagues research the gastrin-releasing peptide receptor–targeting potential of a radiolabeled NOTA-conjugated bombesin derivative in small-animal studies. ***Page 947***

Affinity of Affibody molecules: Tolmachev and colleagues evaluate the effects of human epidermal growth factor receptor 2 (HER2) affinity, binding site composition of HER2-binding Affibody molecules, and HER2 density on tumor targeting. ***Page 953***

Radiocopper imaging for Wilson disease: Bahde and colleagues use a ^{64}Cu-labeled PET agent to successfully identify *Atp7b*-dependent biliary copper excretion, with potential for advancing molecular imaging in Wilson disease. ***Page 961***

Radiofluorinated 5-HT$_{1A}$ agonist: Lemoine and colleagues describe the development of the high-affinity 5-HT$_{1A}$ receptor agonist ^{18}F-F13714 and investigate its utility for PET brain imaging of the serotonin 1A receptor. ***Page 969***

Attenuation correction in PET/MRI: Marshall and colleagues detail a technique to incorporate patient-specific lung density information into MRI-based attenuation maps and compare this with approaches that assume uniform lung density. ***Page 977***

^{18}F-choline biokinetics and dosimetry: Giussani and colleagues detail a compartmental biokinetic and dosimetric model for ^{18}F-choline in the differential diagnosis of prostate cancer and its recurrence. ***Page 985***

PET and iNOS: Herrero and colleagues describe an ^{18}F-labeled inducible form of nitric oxide synthase and report on initial studies and dosimetry in patients after orthotopic heart transplantation. ***Page 994***

ON THE COVER

The recently introduced first integrated whole-body PET/MRI scanner has been shown to give results comparable to PET/CT in a clinical setting. In the patient shown here, with metastasized thyroid carcinoma, a comparison of PET/CT and PET/MRI data acquired on the same day shows an overall similarity in the pattern of suspected lesions. PET/MRI may offer new opportunities in oncologic diagnostics.

See page 849.